COBEM 2021 26th International Congress of Mechanical Engineering
November 22-26, 2021, Virtual Congress, Brazil

COB-2021-2116
INVESTIGATION OF THE INFLUENCE OF LOADING ON THE WEAR OF A PERLITIC RAIL

Vinicius Silva dos Reis
Eric Elian Lima Espíndola
UFPA – Federal University of Pará – Rua Augusto Corrêa, 01 – Guamá. CEP 66075-110. Belém – Pará – Brazil
e-mail: vsdosr@gmail.com
e-mail: ericesp53@gmail.com

Aélcio de Jesus Monteiro dos Santos
UFPA – Federal University of Pará – Rua Augusto Corrêa, 01 – Guamá. CEP 66075-110. Belém – Pará – Brazil
e-mail: aélcio.ms@hotmail.com

Mateus José Araújo de Souza
UFPA – Federal University of Pará – Rua Augusto Corrêa, 01 – Guamá. CEP 66075-110. Belém – Pará – Brazil
e-mail: Mateusjose1903@gmail.com

Carlos Vinícius de Paes Santos
UFPA – Federal University of Pará – Rua Augusto Corrêa, 01 – Guamá. CEP 66075-110. Belém – Pará – Brazil
e-mail: carlosviniciusdepaessantos@gmail.com

José Maria do Vale Quaresma
UFPA – Federal University of Pará – Rua Augusto Corrêa, 01 – Guamá. CEP 66075-110. Belém – Pará – Brazil
e-mail: quaresma@fem.unicamp.br

Abstract. *Brazil still does not exploit this means of rail transport satisfactorily. Thus, it is interesting to study this type of system and its mechanical characteristics. This work aimed to characterize a pearlitic matrix rail as to the parameters of hardness, wear resistance and roughness. The rail was subjected to a pin-on-disk wear test in two loading conditions (50 and 100 N) and after the end of these tests the surfaces were analyzed via SEM, in addition to the roughness parameters in a 3D optical profilometer. The variation of loads altered wear-related properties (hardness, mass loss, wear rate, and coefficient), since there was an increase in hardness when compared to the surface hardness of the rail in a proportional manner to the applied loads. In turn, the wear coefficient also suffered variations associated with the loads, as did the roughness parameters. As for the average coefficient of friction, no significant changes occurred due to the variation in loads. The analysis of the worn surface of all conditions revealed that the wear was moderate and of the oxidative type. Finally, the effects of loading enabled the understanding of the wear mechanisms in the tribological interactions of the rails.*

Keywords: *Wheel-rail contact, Wear, Roughness, Pearlitic steel*

1. INTRODUCTION

Railroads, as well as many other modes of transportation, suffer from wear-related failures. This situation is worrisome due to the range of products that are transported by railroads and, among them, minerals and grains stand out. Generally, as these cargos demand high loadings, they seek to increase speeds (Viáfara, 2005). By increasing the axle load, it is possible to reduce the quantity of trainsets and, consequently, the cost (Chaves, 2017). As a consequence of the search to increase the load carried, in this type of activity, seeking to promote greater competitiveness and decrease logistics costs, the rails employed are subject to severe cycles of efforts (Masoumi, Sinatora, and Goldenstein, 2019).

In the global industry, one of the biggest concerns is the wear and tear of equipment, since it is the most frequent cause of failure of machinery or part of it, which causes losses due to unexpected downtime, maintenance, and replacement. Wear is presented in different types, the most frequent being abrasion wear, erosion wear, sliding wear, and contact fatigue wear (Deutsches Institut für Normung, 1997).

The rails are materials that go through relatively severe service conditions, since they are subject to shocks, alternating bending stresses and wear, the latter being sometimes of concern, since this mechanical element composes the superstructure of the railway track, besides being the rolling surface for the wheels of the railway vehicles, and has been undergoing permanent evolutions with regard to the development of steel technology (Brina, 1988; Chiaverini, 1977). The ends of the rails must be designed so that they can suffer the shock of the wheels of the trainsets when they pass through the joints that will join one rail to another (Chiaverini, 1977).

Rails with pearlitic microstructure, that is, with lamellar structure, have been widely used due to their good mechanical strength, ductility, and economic factors (Masoumi, Sinatora; Goldenstein, 2019; Maya-Johnson, Ramirez; Toro, 2015). AISI H13 is a hot worked steel that contains chromium, molybdenum, and vanadium. It is classified as a tool steel with high hardenability and excellent toughness that is routinely used to make dies, extrusion mandrels, plastic molds, cores, mold holder blocks, and hot working punches (Telasang; Dutta Majumdar; Padmanabham, 2015; Roberts, Kennedy; Krauss, 1998).

Friction force originates from microscopic interactions between surfaces that are in mechanical contact and slide against each other (Bhushan, 2013). This definition encompasses two important classes: sliding and rolling. This force is tangential to the contact interface and with a direction opposite to that of sliding. In both ideal sliding or rolling motions, the tangential force F is required to move a body against the surface of another stationary body. The ratio between this frictional force and normal load W is known as the coefficient of friction, which is usually represented by μ.

When one wear surface slides over the other, wear will occur on one or both of them (Hutchings; Shipway, 2017). The definition of sliding wear is related to the type of contact, thus, not characterizing a wear mechanism in the scientific view (Bhushan, 2001), however, it can be caused by wear mechanisms cited by Zum Gahr (1987): adhesion, abrasion, surface fatigue and tribochemical reactions.

In view of this, it is evident that several factors can contribute to the performance of wheel-rail systems, and the analysis of microstructures and the predominant wear mechanisms significantly helps in the selection of the rails that can be used to perform in various types of railway lines, especially those that have high load rates associated with gradually increasing speeds. Such factors can act as a guide and assist in making a decision as to which type of rail should be purchased.

2. MATERIALS E METHODS

2.1 Obtaining the pins and disks

The TR68 rails used in this work were provided by a company that operates railroads and are classified as heavy haul. The components came cut lengthwise, however, the part of the rail to be analyzed is the billet. Figure 1 shows the rails as received and used.

Figure 1. Rail as received. Source: Author

The rail, more specifically the billet region of one of the rails present, was cross-cut so that the thickness was sufficient to allow the chemical analysis to be performed via optical spectroscopy.

The pins are 20 mm long and 5 mm in diameter. The scheme for the removal of the pins, as well as more details regarding its geometry, is shown in Fig. 2. In order to guarantee replicability, three (3) pins were removed for each load used in the pin-on-disk tests. In addition, at least two (2) pins obtained were used to obtain samples, by successive cuts via cut off.

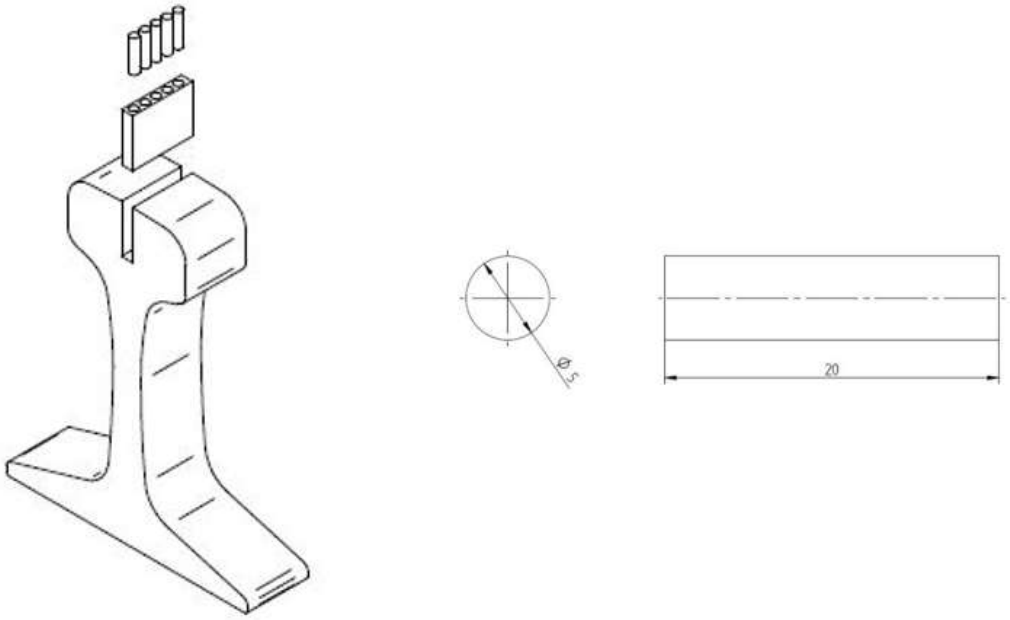

Figure 2. Arrangement and dimensions of the removed pins in drawing without scale and dimensions in mm. Source: Author. Adapted from (Almeida *et al*., 2019).

ABNT H13 steel discs, the discs have a diameter of 76 mm, with a concentric hole of 8.1 mm and a thickness of 4 mm. According to Santos (2013), originally acquired in round bar format in the hardened condition with a hardness around 440 HV. In view of this, they were cut and underwent heat treatments (quenching associated with tempering) in order to obtain hardness levels of 380 and 600 HV (≈ 39 and ≈ 54 HRC).

2.2 Microhardness

The microhardness was obtained using the HV-1000B digital microhardness meter, shown in Figure 3. To measure this property, a quantity of 120 indentations was performed, with 30 indentations, in each quadrant with a load of 50g for a period of 30s. This practice is in compliance with the standard (AMERICAN SOCIETY FOR TESTING AND MATERIALS, 2005a).

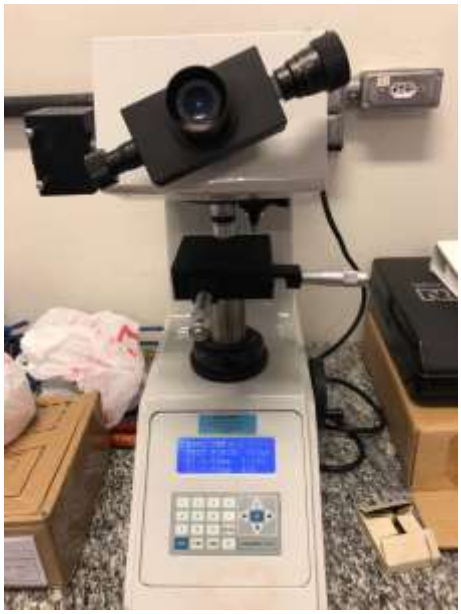

Figure 3. Digital Microdurometer. Source: Author.

2.3 Pin on disc test

The pin-to-disk test was conducted, considering the ASTM G99-05 standard (AMERICAN SOCIETY FOR TESTING AND MATERIALS, 2005b), making use of pins and disks. The pin-on-disk tests were carried out in a TE67 Tribometer – PLINT, Fig. 4a. The loads adopted to carry out the tests were 50, 100 N. Therefore, normal tensions of the order of 2.54, 5.09 MPa were reached. It is noteworthy that, for each load, 3 (three) pins were tested.

The other conditions adopted were similar to the literature (TRESSIA et al., 2020; MASOUMI et al., 2019). Therefore, the following parameters were adopted: the rotation speed was 75 rpm, the sliding track radius of 25 mm, the sliding speed reached is 0.2 m/s and the test time was 3600 seconds for each pin, so the distance slipped was equivalent to 720 m. The test scheme was similar to that shown in Fig. 4b.

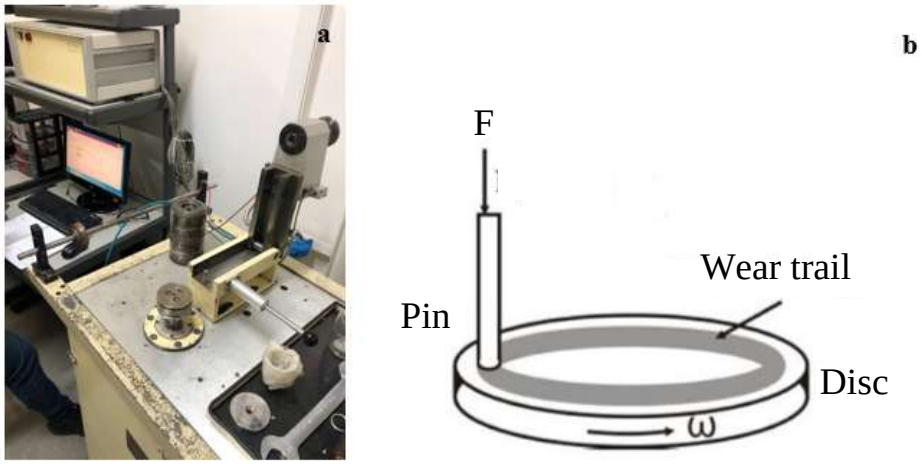

Figure 4. Tribometer for carrying out the pin-under-disk test and test performance scheme. Source: (a) Author and (b) adapted from (SANTOS, 2013).

The mass of the pins was measured, before and after carrying out the tests, so that the loss of mass could be verified; It is important to point out that the pin, before being weighed, must undergo a demagnetization procedure. Weighing was performed on a METTLER TOLEDO AB 204 Analytical Scale belonging to LSF/USP.

2.4 Scanning Electron Microscopy (SEM)

The acquisition of images and analysis via EDS was performed in a Scanning Electron Microscope (SEM), brand TESCAN, model Mira3, with electron gun type FEG and EDS, model PentaFet X-Act, manufactured by Oxford, belonging to the Laboratory of Electronic Microscopy of the Museu Paraense Emílio Goeldi. In this equipment, images were obtained for the investigation of worn surfaces. Figure 5 shows the equipment used to capture the images.

Figure 5. Scanning Electron Microscope. Source: Author.

2.5 Determination of roughness parameters

The surface topography of the samples (pins and discs) was analyzed by a 3D CCI profilemeter manufactured by Taylor Hobson, that is, the 2D and 3D parameters were obtained. To analyze the surface roughness, digital images of the surface of the discs and pins were generated using the software Talymap® (Digitalsulf). The data obtained by the equipment were treated using the standards ISO 4287 (Geometrical Product Specifications) and ISO 25178 (Geometrical product specications (GPS) – Surface texture: Areal). Figure 6 shows the equipment used to determine topographic characteristics.

Figure 6. CCI 3D profilometer. Source: Author

3. RESULTS AND DISCUSSIONS

3.1 Wear

This section will discuss the results of the sliding tests, for the two loads of 50, 100 N, which corresponded to F1 and F2, respectively.

3.1.1 Mass loss and wear coefficient

The mass losses for the pins and discs, as well as the coefficient and wear rate, as a function of the test conditions (F1 and F2), are presented in Table 1.

Table 1. Mass loss and wear coefficient. Source: Author.

Normal force [N]	Loss of disk mass [mg]	Pin mass loss [mg]	Pin wear rate [mm^3/m]	Pin wear coefficient [K_A]
F1	14.67±8.09	5.72±0.34	$1.01x10^{-3}$	$7.26x10^{-2}$
F2	34.58±2.22	9.27±0.64	$1.64x10^{-3}$	$5.88x10^{-2}$

Regarding the pins, softer, the wear occurred in a moderate regime for all conditions. Figure 7 presents the behavior of the pin, regarding the relevant characteristics for a synthesized mode wear analysis.

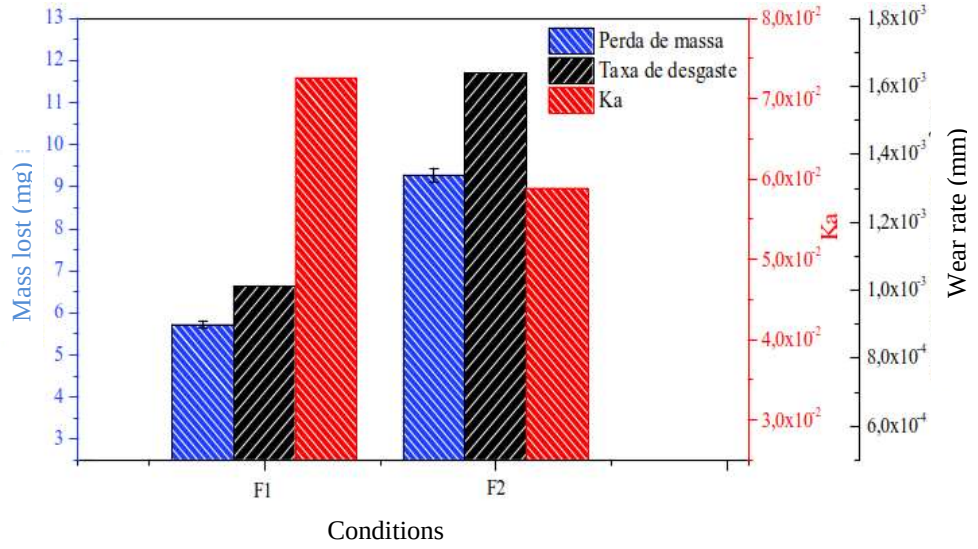

Figure 7. Comparison of the wear parameters of F1 and F2 conditions. Source: Author.

By wear rate one can check the lost pin volume. In both F1 and F2 there was a decrease and, consequently, it can be determined what was the linear reduction in terms of height. Through this analysis, it can be seen that there was no significant reduction in the pin height.

3.1.2 Effect of wear on work hardening

Figure 8 shows how the pins behaved when subjected to the two loading conditions. In the condition as received (CR), the rail presented hardness of 369 HV. As pointed out in the literature (Santos, 2013; Viáfara; Sinatora, 2009), with increasing loading, there is greater work hardening on the surface of the pins.

Comparing CR with conditions F1 and F2 it is noted that there was a variation in hardness of about 20% and 55% the hardness values achieved by the pins at the end of the wear tests were approximately, 453.49±3.72 HV and 568.34±4.26 HV. Figure 8 presents the hardness values measured, as well as the increase in strain hardening, with the standard rail hardness as reference.

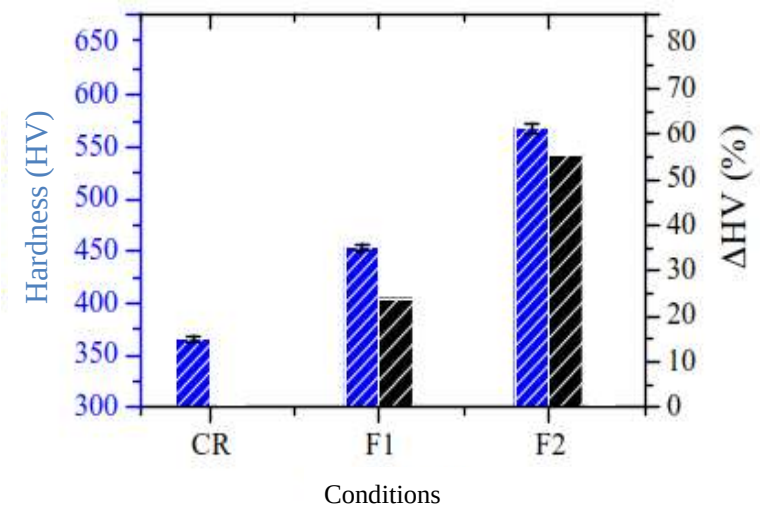

Figure 8. Variation of the hardness and hardness of the pins. Source: Author.

3.1.3 Analysis of the coefficient of friction

Next in Figure 9 are the variation curves, of coefficient of friction, for conditions F1 and F2. The test time and sliding distance were 3600 s and 720 m, respectively. The curves have the most typical behavior, since at the beginning of the contact, due to the surface roughness, the friction becomes increasing, creating a peak, until conformity and reduction of friction occurs. Thus it can be said that these characteristics are of lubricated or even non-lubricated sliding of metals, as

in the case of steel on steel pair, Viáfara (2005) points out that, in the case of the F2 condition in pins with pearlitic microstructure, the presence of oxides such as Fe_3O_4 and Fe_2O_3 can occur.

The latter is, has its formation characterized in most cases by high temperatures and/or loadings and acts preventing the metallic contact between the surfaces and, with this, inducing the moderate regime of oxidative wear. It is noted that in condition F1 the running-in period extends until approximately 500 s, after which a stage of stabilization of the friction coefficient begins, a fact that was also observed by Tressia *et al*., (2020) in test conditions very similar to those adopted in this work.

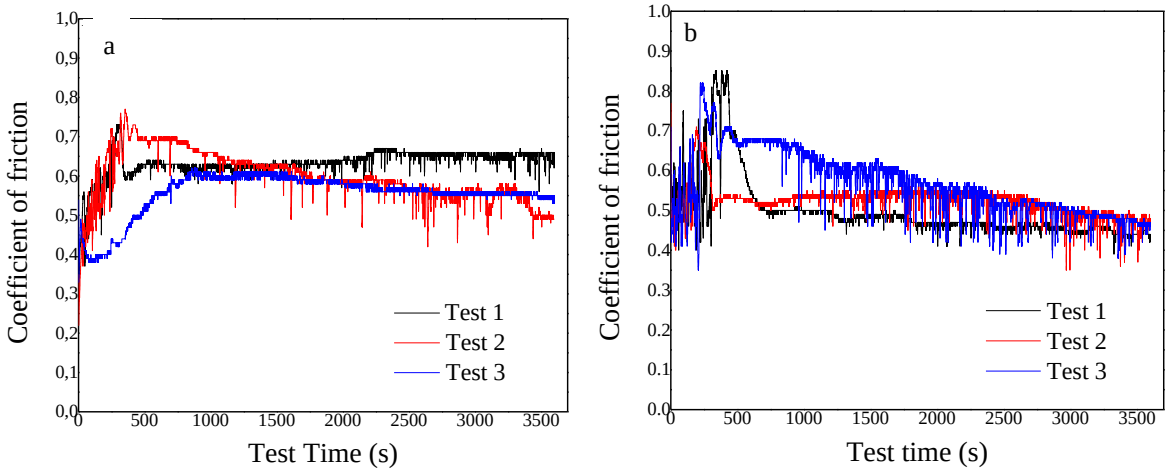

Figure 9. Variation of friction coefficient with sliding distance for conditions (a) F1, (b) F2 N. Source: Author.

3.1.4 Analysis of wear surface

Figure 10 shows the scanning electron microscopy images of the wear tracks. Taking an overview, it can be seen that in condition F1 (50 N) and F2 (100 N), in addition to abrasion marks, adhesion points appear. The adhesion points were also verified in other literature (Viáfara, 2005; Tressia *et al*., 2020) that performed sliding wear on pins with pearlitic structures.

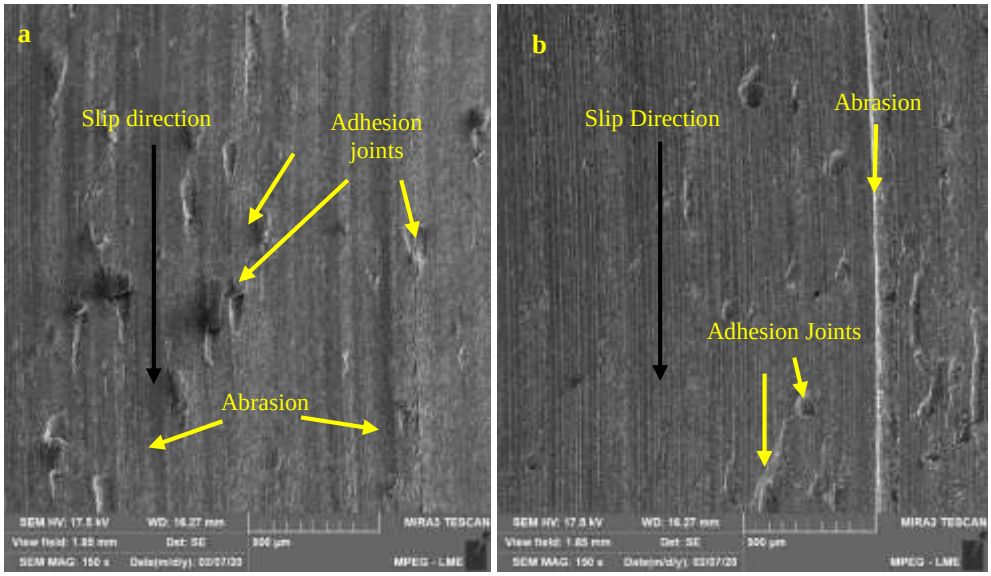

Figure 10. Secondary electron scanning electron microscopy images of the worn surface tracks for (a) F1 and (b) F2 conditions. Source: Author.

3.2 Analysis of the roughness parameters

Table 2 shows the roughness parameters (Rq, Ra, Rv and Rsk), for the discs and pins tested under conditions F1 and F2.

Table 2. R roughness parameters of the disc wear trails for F1and F2 conditions. Source: Author.

Condição	TS	Rq (µm)	Ra (µm)	Rv (µm)	Rsk
F1	Disk	1.61± 0.17	1.23± 0.06	2.40± 0.19	-0.37± 0.24
	Pin	1.92	1.40	2.84	-0.16
F2	Disk	2.16± 0.15	1.62± 0.21	2.28± 0.41	-0.24± 0.26
	Pin	2.21	1.62	3.08	0.02

The analysis of the table shows the increase of the roughness parameters, given also the increase of the normal loads, applied during the pin-on-disk test. The parameters Ra and Rq complement each other analytically, since both indicate the height of the surface, however, Rq is more reliable, so it can be seen that, for the conditions analyzed, both have increasing behavior with increasing load, indicating greater variations in the roughness profile. The Rv parameter indicates the maximum depth of the valleys of the samples, a fact that indicates increasing depth with the increase of the normal load for the pins and, in the case of the discs, there is little variation when comparing the F1 and F2 conditions.

It is observed that the Rsk parameter remains with negative values for the disks and, for the pins, this pattern is modified, that is, in the F2 situation, the value becomes positive. The negative Rsk parameter indicates that the surface has low peaks and deep valleys, thus the increase in load evidences, for the discs, a tendency to remove peaks and increase the depth of the valleys. In comparison with the work of Santos (2013), which presented a lower growth trend of the roughness parameters for the pair pin (340 HV) and disk (600 HV), it can be stated that this variation is different from the situation studied for the pair: pin (Rail) and disk (H13), in which there was a notorious variation. Such differentiation is due to the parameters used in the wear, as well as the type of steel, since, in the cited work, the 4140 steel was used.

The topographical images, obtained by the 3D profilometer for 2 (two) quadrants of each disc tested in conditions F1 and F2, are exposed in Fig. 11. It can be seen that the effect of the variation of the load condition was notorious on the worn surfaces of the discs.

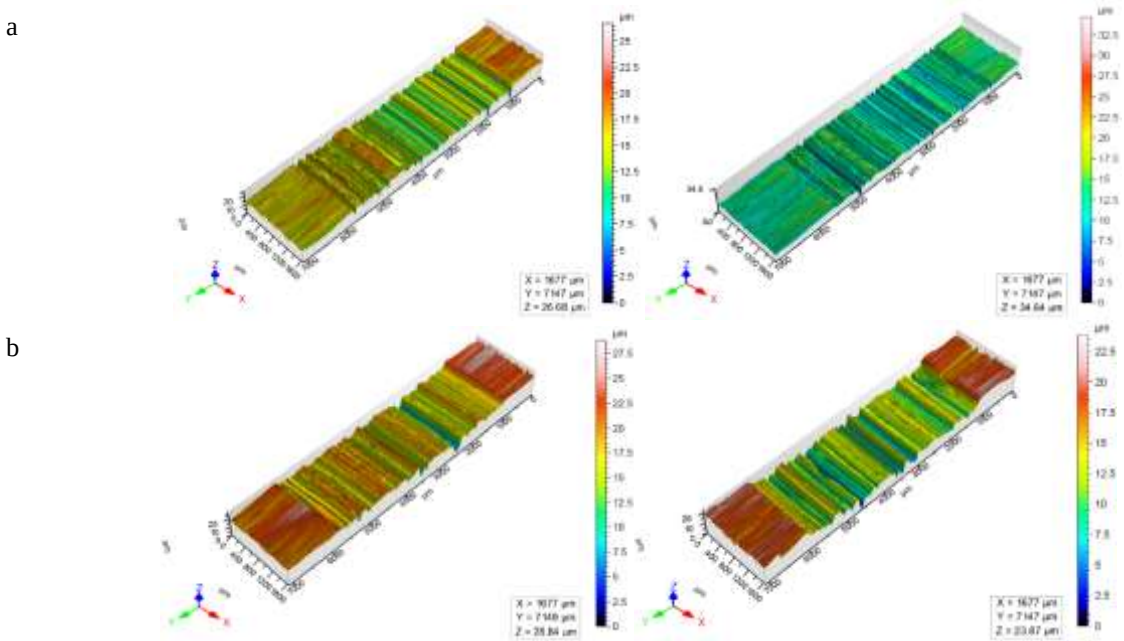

Figure 11. Images of the stitches of the quadrants measured for the disks in the (a) F1, (b) F2 conditions. Source: Author.

The images of the topographies of the 3D profiles, obtained by the 3D profilometer, for the worn pins are presented in Fig. 12, for conditions F1 and F2. The wear trail of the pins points out that for the conditions of this system, there are clear changes in the worn surface, which can be noticed with the trend of increasing roughness. Furthermore, it is

noticeable that the topographies indicate various appearances of adhesion marks, highlighted by their depth on the surfaces, as the forces change.

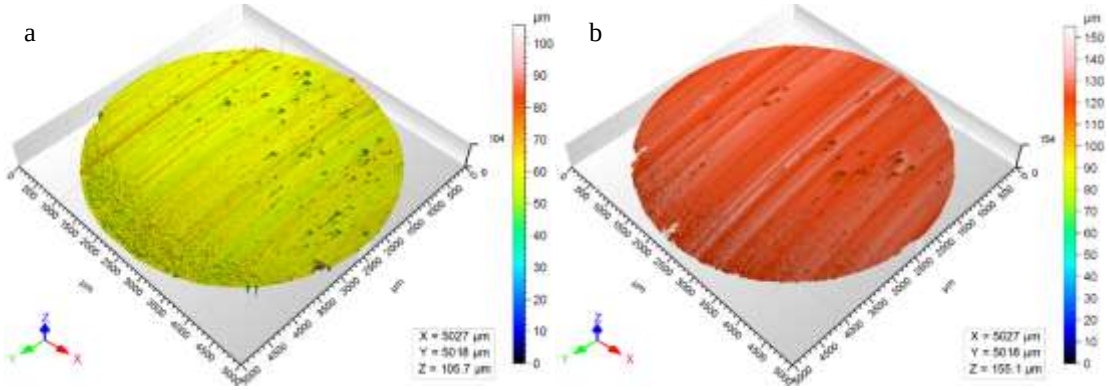

Figure 12. Images of the measured quadrant stitches for the pins in the (a) F1, (b) F2 conditions. Source: Author

4. CONCLUSIONS

As for the evaluation of the wear resistance for the surface, when subjected to the loadings of 50, 100 N, it can be seen that there is an increase in the wear rate and mass loss until the load of 100N. The wear coefficients indicate that the wear was moderate for all loading conditions. The variation in the average coefficient of friction was not significant at all proposed loadings. The roughness parameters R, as well as the analysis of the topographies showed that there are appreciable differences of the pin and disc surfaces when submitted to the different loadings and, in turn, the eventual formation of the oxide layer motivated variations in the shape and depth of the valleys and peaks.

5. ACKNOWLEDGEMENTS

The authors thank the Federal University of Pará for the infrastructure support, as well as the Laboratory of Surface Phenomena at USP for the access to the tribological equipment.

6. REFERENCES

American Society for Testing and Materials, 2005a. “ASTM E384: Standard Test Method for Knnop and Vickers Hadness of Materials”. *ASTM International. [S.l.]*.

American Society for Testing and Materials, 2005b. “ASTM G99-05: Standard Test Method for Wear Testing with a Pin-on-Disk Apparatus”. *ASTM International. [S.l.]*.

Bhushan, B, 2001. *Modern tribology handbook. 1. Principles of tribology*. [S.l.]: CRC press.

Bhushan, B, 2013. *Introduction to tribology. [S.l.]: John Wiley & Sons*.

Blau, P. J, 2005. “On the nature of running-in. Tribology international”. Vol. 38, No. 11-12, pp. 1007-1012.

Brina, H. L, 1988. “Railways” (in Portuguese). *Belo Horizonte: Editora UFMG*, Vol. 1, No. 2.

Chaves, A. P. G, 2017. “Railroad wheels: analysis, microstructure and improvement proposals”. Master’s Thesis, Master in Engineering) - University of São Paulo. São Paulo, Brazil.

Chiaverini, V. *Cast iron and steels* (in Portuguese). *[S.l.]: Abm*, 1977.

Deutsches institut für normung, 1997. *DIN 50320: Systematic analysis of wear processes: classification of wear phenomena* (in Portuguese). *Metalurgia & Materiais*. [S.l.].

Hutchings, I.; Shipway, P, 2017. *Tribology: friction and wear of engineering materials. [S.l.]: Butterworth-Heinemann*.

Masoumi, M.; Sinatora, A.; Goldenstein, H, 2019. “Role of microstructure and crystallographic orientation in fatigue crack failure analysis of a heavy haul railway rail”. *Engineering Failure Analysis*, Vol. 96, pp. 320-329.

Maya-johnson, A.; Ramirez, A. J.; Toro, A. “Fatigue crack growth rate of two pearlitic rail steels”. *Engineering Fracture Mechanics*, Vol. 138, pp. 63-72.

Roberts, G. A.; Kennedy, R.; Krauss, G, 1998. *Tool steels. [S.l.]: ASM international*.

Santos, E. D. C, 2013. “Effect of the hardness of a harder body on the coefficient of friction, surface roughness and wear resistance of a steel x steel pair as a function of normal load variation”(in Portuguese). Master’s Thesis, Master in Mechanical Engineering) - Federal University of Pará. Belém, Brazil

Viáfara, C. C. C. J. M. V. A. T, 2005. ”Unlubricated sliding wear of pearlitic and bainitic steels”. *Wear*, Vol. 259, pp. 405-411.

Viáfara, C. C.; Sinatora, A, 2009. “Influence of hardness of the harder body on wear regime transition in a sliding pair of steels”. *Wear*, Vol. 267, No. 1-4, pp. 425-432.

Telasang, G.; Dutta Majumdar, J.; Padmanabham, G, M. I, 2015. “Wear and Corrosion Behavior of Laser Surface Engineered AISI H13 Hot Working Tool Steel”. *Surface & Coatings Technology*, Vol. 261, pp. 69-78.
Tressia, G. et al, , 2020. ”Improvement in the wear resistance of a hypereutectoid rail via heat treatment”. *Wear*, Vol. 442, pp. 203122.
Zum Gahr, K.-H, 1987. *Microstructure and wear of materials. [S.l.]: Elsevier*.

7. RESPONSIBILITY NOTICE

The authors are the only responsible for the printed material included in this paper.